

Annealing temperature and thickness dependencies of structural and magnetic properties of Co₂FeAl thin films

M. Belmeguenai,^{1,*} M. S. Gabor,^{2,†} F. Zighem,¹ Y. Roussigné,¹ D. Faurie,¹ and C. Tiusan^{2,3}

¹*LSPM-CNRS, Université Paris XIII-Sorbonne Paris Cité, F-93430 Villetaneuse, France*

²*Center for Superconductivity, Spintronics and Surface Science, Technical University of Cluj-Napoca, Strada Memorandumului No. 28, RO-400114 Cluj-Napoca, Romania*

³*Institut Jean Lamour, CNRS, Université de Nancy, BP 70239, F-54506 Vandoeuvre, France*

(Received 20 May 2016; revised manuscript received 5 September 2016; published 22 September 2016)

Co₂FeAl (CFA) thin films, of various thicknesses ($3 \text{ nm} \leq t \leq 50 \text{ nm}$), have been grown by sputtering on (001) MgO single-crystal substrates and annealed at different temperatures ($RT \leq T_a \leq 600^\circ\text{C}$, where RT is the room temperature). The influence of the CFA thickness (t), as well as *ex situ* annealing temperature (T_a), on the magnetic and structural properties has been investigated by x-ray diffraction (XRD), vibrating sample magnetometry, and broadband microstrip ferromagnetic resonance (MS-FMR). The XRD revealed an epitaxial growth of the films with the cubic [001] CFA axis normal to the substrate plane and that the chemical order varies from the *B2* phase to the *A2* phase when decreasing t or T_a . The deduced lattice parameters showed an in-plane tetragonal distortion and in-plane and out-plane strains that increase with T_a and $1/t$. For all T_a values, the variation of the effective magnetization, deduced from the fit of MS-FMR measurements, shows two different regimes separated by a critical thickness, which is T_a dependent. It decreases (increases) linearly with the inverse thickness ($1/t$) in the first (second) regime due to the contribution of the magnetoelastic anisotropy to surface (to volume) anisotropy. The observed behavior has been analyzed through a model allowing for the separation of the magnetocrystalline, magnetoelastic, and Néel-type interface anisotropy constants to the surface and the volume anisotropies. Similar behavior has been observed for the effective fourfold anisotropy field which governs the in-plane anisotropy present in all the samples. Finally, the MS-FMR data also allow one to conclude that the gyromagnetic factor remains constant and that the exchange stiffness constant increases with T_a .

DOI: [10.1103/PhysRevB.94.104424](https://doi.org/10.1103/PhysRevB.94.104424)

I. INTRODUCTION

Materials with high spin polarization, such Heusler alloys [1–3], are eligible for spintronic applications. These materials are considered as a key technology to solve some spintronic challenges, especially large magnetoresistance ratios, low critical current densities for spin transfer torque magnetization switching [4], and the injection and the detection of spin-polarized currents from metallic ferromagnets into semiconductors. Among the full Heusler alloys, Co₂FeAl (CFA) is a very attractive material due to its high Curie temperature ($T_C \approx 1000 \text{ K}$) [5] and its relatively high spin polarization leading to high tunnel magnetoresistance (TMR) ratios up to 360%, as achieved in CoFe/MgO/Co₂FeAl structures [6,7]. In addition to its lowest magnetic damping parameter among Heusler compounds [8], making it suitable for magnonic [9] devices, the relatively small lattice mismatch between MgO(001) and CFA(001) enables the fabrication of high quality CFA/MgO(001) epitaxial heterostructures with low resistance area product magnetic tunnel junctions (MTJs) [10], which are essential for spin transfer switching [11]. However, in such alloys, there is always some degree of chemical disorder, which strongly influences many of their physical properties. In reality, the totally ordered phase (*L2*₁) is difficult to achieve and there are a variety of possible disorder types. When Co atoms are completely ordered while disorder occurs only between Fe and Al atoms, the *B2* structure is

obtained. The structure *A2* corresponds to a complete disorder between all atoms Co, Fe, and Al. It was reported by Picozzi *et al.* that some types of disorder in Heusler alloys might lead to additional states at the Fermi level, thus reducing the spin polarization [12]. In addition to the atomic order, the crystallographic orientation of the Heusler thin film is important. The (001) texture of the Co-based Heusler film is essential for single-crystal MTJs based on these materials and (001) MgO tunnel barriers, where tunneling polarization could be particularly large due to the symmetry-dependent attenuation rate of the propagative Bloch function selected in single-crystal ferromagnetic electrodes [13]. Moreover, in (011) textured Heusler compounds, the Co atoms at the interface may reduce spin polarization. Therefore, an annealing process is required to initiate crystallization and to induce atomic ordering. It is thus of great interest to investigate the effect of annealing temperature (T_a) on the structural and magnetic properties of CFA thin films. Furthermore, we recently showed that CFA thin films (with a thickness down to 10 nm) grown on MgO substrates exhibit a strong negative perpendicular anisotropy (reinforcing the in-plane easy plane). This turns out to be a purely interfacial contribution [8]. Therefore, it is of great interest for both fundamental and technological reasons to investigate the magnetic behavior of the CFA ultrathin films (with a thickness down to 2 nm) grown on MgO and to point out the annealing temperature dependencies of the interfacial anisotropy over a large range of CFA thicknesses, in order to allow for the manufacturing of CFA films with the desired properties. The experimental strategy employed in this paper is a complex correlated structural, static, and dynamic magnetic analysis. Therefore, the x-ray diffraction

*belmeguenai.mohamed@univ-paris13.fr

†mihai.gabor@phys.utcluj.ro

(XRD), ferromagnetic resonance in microstrip line (MS-FMR) under in-plane applied magnetic field, combined with vibrating sample magnetometry (VSM) allowed us to correlate the structural and magnetic properties of CFA thin films grown on MgO substrates and annealed at different temperatures. Our results demonstrate the presence of in-plane and perpendicular to the plane interface anisotropies, which are T_a dependent and their signs depend on the CFA thickness, offering the possibility of versatile sample design with skillfully tuned magnetic properties.

II. SAMPLE PREPARATION AND EXPERIMENTAL METHODS

CFA films were grown on MgO (001) single-crystal substrates using a magnetron sputtering system with a base pressure lower than 4×10^{-9} Torr. Prior to the deposition of the CFA films, a 5 nm thick MgO buffer layer was grown at room temperature (RT) by rf sputtering from a MgO polycrystalline target under an argon pressure of 15 mTorr. The role of this MgO buffer layer is to improve the flatness quality of the substrate and to trap the residual carbon, thus preventing carbon diffusion across the stack during the annealing stages. Next, the CFA films, with variable thicknesses ($t = 50, 30, 15, 10, 7.5, 5,$ and 3 nm), were deposited at RT by dc sputtering under an argon pressure of 1 mTorr, at a rate of 0.1 nm/s. Finally, CFA films were capped with a 5 nm thick MgO layer. After the growth of the stack, the structures were *ex situ* annealed at different temperatures ($T_a = \text{RT}, 200^\circ\text{C}, 300^\circ\text{C}, 400^\circ\text{C}, 500^\circ\text{C},$ and 600°C) for 60 min in vacuum (with a pressure lower than 3×10^{-8} Torr).

III. RESULTS AND DISCUSSIONS

A. Structural properties

In order to determine the crystal structure and chemical order degree of the CFA films, we have performed x-ray diffraction experiments. Figure 1(a) shows typical 2θ - ω diffraction patterns for the 50 nm film as functions of the annealing temperature. One can observe that, besides the peak corresponding to the MgO substrate, the patterns only show the (002) and (004) CFA peaks. The (002) superlattice peak is characteristic of the $B2$ phase of CFA and, therefore, the absence of this peak is a signature of the $A2$ phase in which Fe, Al, and Co randomly occupy the atomic sites. Since the (004) reflection is a fundamental one corresponding to the cubic CFA structure, the ratio $A(002)/A(004)$ of the integrated intensities of the (002) and of the (004) peaks, which increases with the film thickness and the annealing temperature, represents the measure of the order degree on the Co sites. This ratio, shown in Fig. 1(b) as a function of T_a for thicker films, increases with T_a above 300°C , suggesting a monotonous enhancement of the chemical order from the $A2$ towards the $B2$ phase as the thickness and T_a increase. For CFA thicknesses below 10 nm, the films present an $A2$ phase for all annealing temperatures.

Using scans of different orientations, we evaluated the out-of-plane (a_\perp) and the in-plane (a_\parallel) lattice parameters as shown in Fig. 1(c) as function of T_a for different film thicknesses. For $t < 5$ nm, the estimation of the lattice parameter was impossible due to the very low signal-to-noise ratio. At low temperatures, a_\perp is higher than a_\parallel , suggesting that the CFA

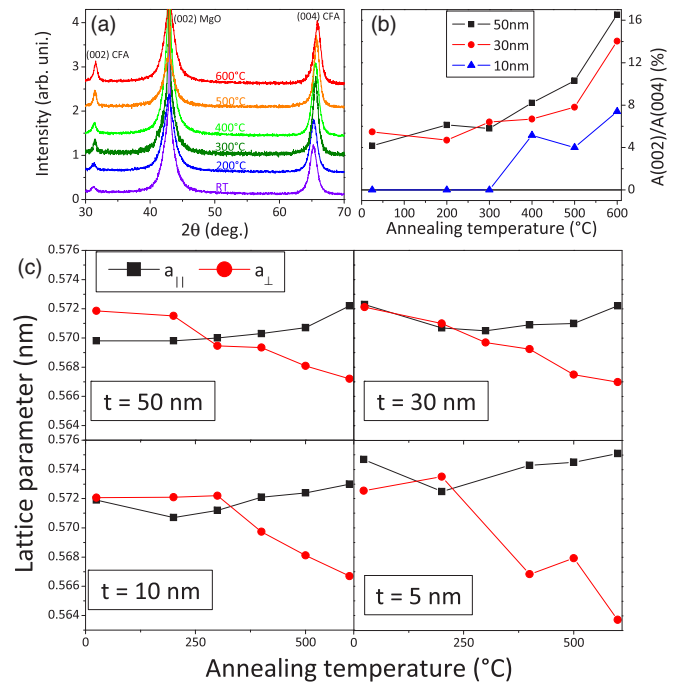


FIG. 1. (a) Typical example of $2\theta/\omega$ (out-of-plane) x-ray diffraction patterns for 50 nm thick CFA films annealed at different temperatures. The patterns have been shifted vertically for better visibility. (b) Evolution of the integral intensities of the (002) and (004) CFA peaks [$A(002)/A(004)$] with respect to the annealing temperature for different film thicknesses t . (c) In-plane and out-of-plane lattice parameter variations as function of the annealing temperature for different film thicknesses. In (b) and (c), symbols refer to measurements while solid lines are guides to the eye.

films experience an in-plane compressive equibiaxial stress. As T_a increases, this stress relaxes: For annealing temperatures around 300°C , the out-of-plane and in-plane lattice parameters show close values. For higher values of T_a , a_\parallel becomes higher than a_\perp , which means that the CFA films are subjected to a tensile in-plane strain that gets more pronounced as T_a increases. A simple elastic model allowed us to derive the unstrained a_0 cubic parameter as well as the in-plane ε_\parallel and the out-of-plane ε_\perp strains:

$$a_0 = \frac{C_{11}a_\perp + 2C_{12}a_\parallel}{C_{11} + 2C_{12}}, \quad \varepsilon_\parallel = \frac{C_{11}}{C_{11} + 2C_{12}} \frac{(a_\parallel - a_\perp)}{a_0},$$

$$\varepsilon_\perp = \frac{2C_{12}}{C_{11} + 2C_{12}} \frac{(a_\parallel - a_\perp)}{a_0}, \quad (1)$$

where the values of the elastic coefficients $C_{11} = 253$ GPa and $C_{12} = 165$ GPa have been previously calculated [14]. For $300^\circ\text{C} < T_a$, the cubic lattice constant a_0 does not possess a clear thickness dependence, as shown in Fig. 2(a). Its value, around 0.570 nm, is slightly smaller than the one reported in the bulk compound with the $L2_1$ structure (0.573 nm) [15]. As T_a decreases, a_0 shows a slight linear variation as a function of $1/t$ [Fig. 2(b)]. The in-plane and out-of-plane strains (ε_\parallel and ε_\perp , respectively), originating from the mismatch with the lattice of the MgO substrate, vary linearly with $1/t$ with a decreasing slope as a function of T_a [Figs. 2(b) and 2(c)]. This slope is negative for $T_a = 300^\circ\text{C}$, vanishes for an annealing

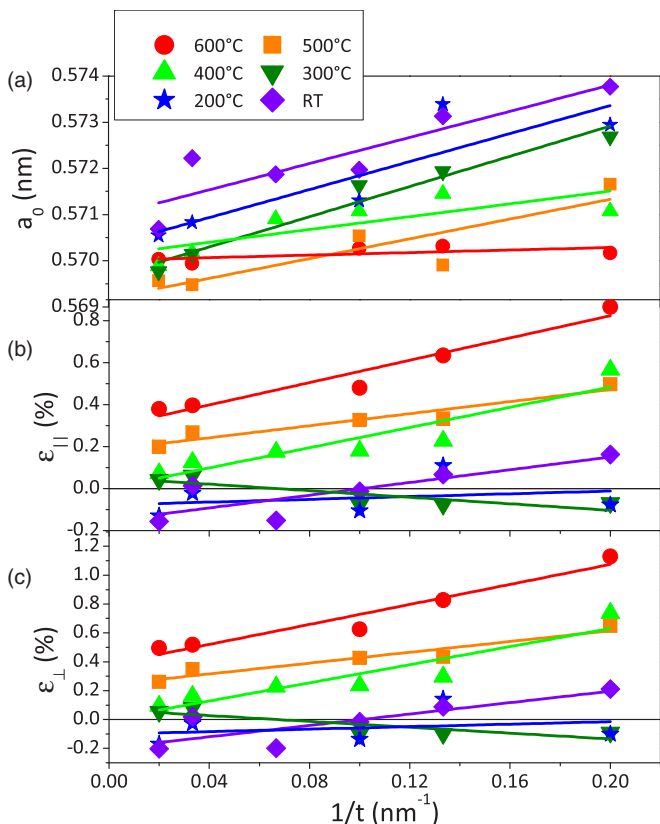


FIG. 2. Thickness dependence of (a) the unstrained cubic lattice parameter a_0 , and (b) the in-plane ε_{\parallel} and (c) the out-of-plane strains ε_{\perp} with the annealing temperature. Symbols refer to measurements and solid lines are linear fits.

temperature of 200 °C, and increases again for the as-deposited samples. The strain values do not exceed a few %, well below the Heusler/MgO mismatch, thus excluding an efficient planar clamping.

B. Static magnetic properties

For all the films studied, the magnetization at saturation has been determined from the hysteresis curves obtained by VSM with an in-plane magnetic field applied along various orientations with respect to the [110] CFA axis. Figure 3(a) shows the CFA thickness dependencies of the saturation magnetic moment per unit area for all annealing temperatures. This dependence is used to determine the magnetization at saturation M_s and the magnetic dead layer t_d . The slope gives the saturation magnetization, while the horizontal axis intercept gives the extent of the dead layer. The annealing temperature dependencies of M_s and t_d are shown in Fig. 3(b). The thickness of the magnetic dead layer remains lower than 0.1 nm for annealing temperatures up to 300 °C, and increases up to 0.27 nm for the samples annealed at 600 °C. This trend is most likely due to the oxidation at the CFA-MgO interface, which becomes more pronounced with increasing annealing temperature. Furthermore, the saturation magnetization of the films shows an increase with annealing temperature, which can be attributed to the improvement of the crystalline quality and of the chemical order with annealing.

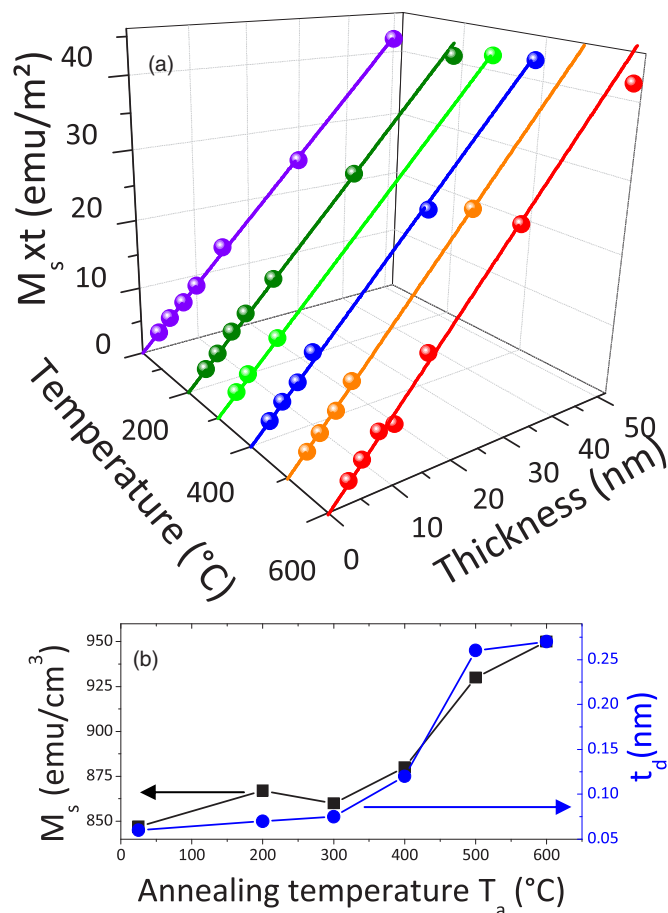


FIG. 3. (a) Three-dimensional (3D) plot of the thickness dependencies of the saturation magnetic moment per unit area for Co_2FeAl thin films annealed at different temperatures T_a . Symbols refer to measurements and solid lines are the linear fits. (b) Variations of the magnetization (M_s) at saturation and the magnetic dead layer (t_d) as function of the annealing temperature of Co_2FeAl thin films. Symbols refer to measurements and solid lines are used as guides to the eye.

C. Dynamic magnetic properties

The MS-FMR spectra, measured for all samples with an in-plane magnetic field applied at different directions φ_H with a respect to the [110] CFA axis (parallel to one of the MgO substrate edges), revealed the existence of the uniform precession mode (UPM). For the 50 nm thick films, it was possible to observe the first perpendicular standing spin wave mode (PSSW). For lower sample thicknesses, the PSSW modes are not detected due to their high frequencies overpassing the available bandwidth (0–20 GHz). The study of the UPM resonance field in dependence of φ_H allows for the determination of in-plane anisotropy constants of thin magnetic films while the resonance field dependencies of UPM and PSSW frequencies give the effective magnetization (M_{eff}), including perpendicular anisotropies and the exchange stiffness constant (A_{ex}). The typical MS-FMR angular dependence of the UPM resonance field at a 10 GHz driven frequency for 5, 10, and 50 nm thick CFA films annealed at different temperatures are shown in Fig. 4. It shows that samples exhibit a clear predominant fourfold magnetic anisotropy superimposed to a small uniaxial anisotropy. The

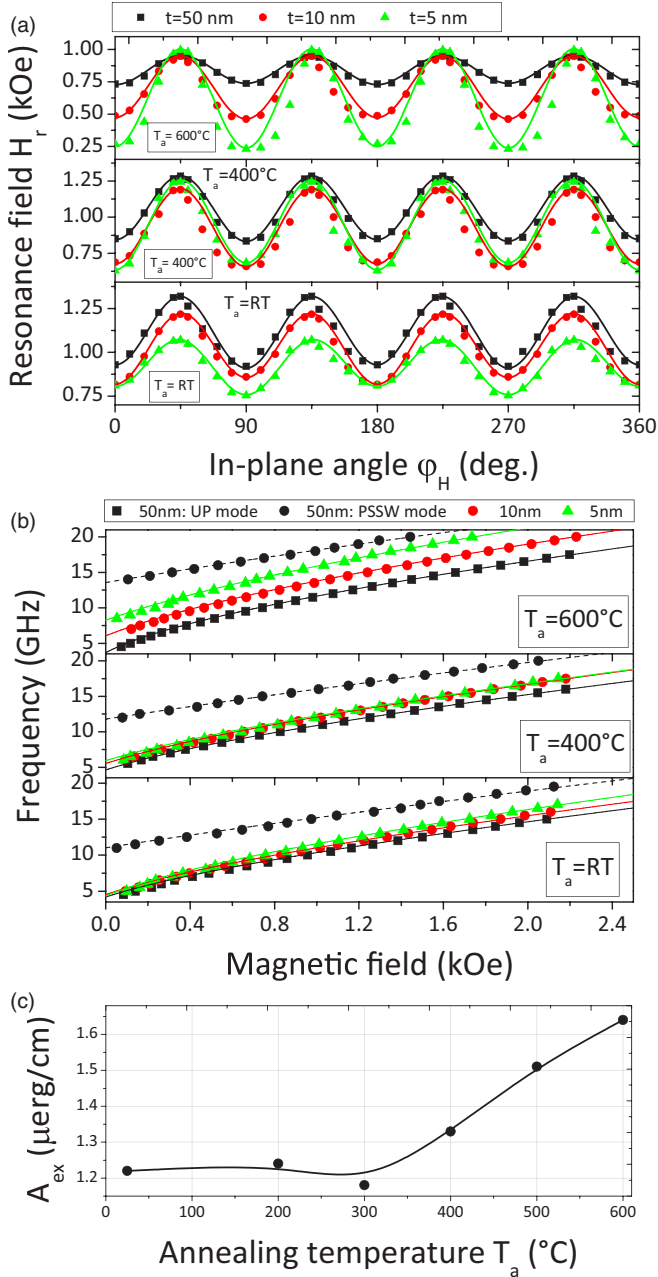


FIG. 4. (a) Angular dependence of the resonance field at a 10 GHz driven frequency for Co_2FeAl films of thickness t . (b) Easy axis field dependencies of the UPM and PSSW mode frequencies. In (a) and (b), solid lines refer to fits obtained using Eq. (1). (c) Variations of the exchange stiffness constant (A_{ex}), as a function of the annealing temperature of Co_2FeAl thin films. Symbols refer to measurements and solid lines are used as guides to the eye.

anisotropy easy axes are straightforwardly deduced from the measurements where the anisotropy directions correspond to the minima of the resonance field. The uniaxial, manifested by different resonance fields at 0° (180°) and 90° (270°), and the fourfold anisotropies have parallel easy axes: Their common axis coincides with one of the substrate edges and, consequently, with the $\langle 110 \rangle$ crystallographic direction of CFA. The epitaxial symmetry of these films, according to the relation $\text{CFA}(001)[110]/\text{MgO}(001)[100]$ [8], agrees with the

principal directions of the fourfold contribution, suggesting a magnetocrystalline origin of the fourfold anisotropy. Moreover, the sinusoidal shape of the angular dependence in Fig. 4 indicates that magnetization and the applied field are collinear for all the angles, suggesting that the resonance field values at this driven frequency are sufficiently high to saturate the magnetization. The corresponding field dependence of the UPM and PSSW mode frequencies recorded for the applied field along the easy axis of CFA thin films are shown in Fig. 4(b).

The experimental data presented here have been analyzed considering the model described in Ref. [8], where the resonance expressions of the uniform precession mode and for the PSSW modes assuming in-plane applied magnetic fields are given by

$$\begin{aligned}
 F_n = \left(\frac{\gamma}{2\pi} \right) & \left\{ \left[H \cos(\varphi_M - \varphi_H) + \frac{2K_4}{M_s} \cos 4(\varphi_M - \varphi_4) \right. \right. \\
 & \left. \left. + \frac{2K_u}{M_s} \cos 2(\varphi_M - \varphi_u) + \frac{2A_{\text{ex}}}{M_s} \left(\frac{n\pi}{t} \right)^2 \right] \right. \\
 & \times \left[H \cos(\varphi_M - \varphi_H) + 4\pi M_{\text{eff}} + \frac{K_4}{2M_s} \right. \\
 & \times [3 + \cos 4(\varphi_M - \varphi_4)] + \frac{K_u}{M_s} [1 + \cos 2(\varphi_M - \varphi_u)] \\
 & \left. \left. + \frac{2A_{\text{ex}}}{M_s} \left(\frac{n\pi}{t} \right)^2 \right] \right\}^{0.5}, \quad (2)
 \end{aligned}$$

where $\gamma/2\pi = g \times 1.397 \times 10^6$ Hz/Oe is the gyromagnetic factor, n is the index of the PSSW, and A_{ex} is the exchange stiffness constant. For the gyromagnetic factor, we showed in previous works [8,16] that it is thickness and annealing temperature independent and its value has been found to be $\gamma/(2\pi) = 29.2$ GHz/T.

In the above expression, φ_M represent the in-plane (referring to the $[110]$ CFA axis) angle defining the direction of the magnetization M_s . φ_u and φ_4 define the angles between the planar uniaxial easy axis and the planar fourfold easy axis with respect to this $[110]$ axis, respectively. K_u , K_4 , and K_\perp are in-plane uniaxial, fourfold, and out-of-plane uniaxial anisotropy constants, respectively. We define $H_u = \frac{2K_u}{M_s}$ and $H_4 = \frac{4K_4}{M_s}$ as the in-plane uniaxial and the fourfold anisotropy fields, and we introduce the effective magnetization $M_{\text{eff}} = H_{\text{eff}}/4\pi$ as

$$4\pi M_{\text{eff}} = 4\pi M_s - \frac{2K_\perp}{M_s}. \quad (3)$$

In this study, the effective perpendicular anisotropy term K_\perp as well as K_4 could be phenomenologically separated in a volume and interfaces contributions and approximately obeying the relations

$$K_\perp = K_{v\perp} + \frac{2K_{s\perp}}{t}, \quad (4)$$

$$H_4 = \frac{4K_{v4}}{M_s} + 4 \frac{2K_{s4}}{M_s t}, \quad (5)$$

where $K_{s\perp}$ (K_{s4}) refers to the perpendicular (in-plane fourfold) anisotropy term of the interfacial energy density and K_{v4} is the fourfold volume anisotropy constant. The CFA layer is

assumed to be bounded by two identical interfaces accounting for the prefactor 2 in the above expressions of K_{\perp} and H_4 .

In this study, the most pertinent magnetic parameters have been obtained as follows: For each sample (of given thickness and annealing temperature), the angular dependence of the resonance field (measured at 10 GHz) and the variation of the frequency of UPM as a function of the applied magnetic field along the easy axis are measured. These data are then conjointly fitted by using Eq. (2) and $\gamma/(2\pi) = 29.2$ GHz/T, allowing for the determination of the in-plane anisotropy fields and $4\pi M_{\text{eff}}$. For the thicker samples (50 nm thick films), where the first perpendicular standing spin wave was observable, the fit of the variation of its frequency as a function of the applied magnetic field along the easy axis allowed for the determination of the exchange stiffness constant A_{ex} , using Eq. (2) and the magnetic parameter determined from the investigation of the UPM (anisotropy fields and $4\pi M_{\text{eff}}$). An example of this procedure is illustrated in Figs. 4(a) and 4(b) where the experimental data and the fits are compared. The obtained A_{ex} , shown in Fig. 4(c), increases versus T_a , presumably due to the enhancement of the chemical order and the crystallization of CFA. A similar behavior of the exchange stiffness of $\text{Co}_2\text{FeAl}_{0.5}\text{Si}_{0.5}$ with T_a has been reported by Trudel *et al.* [17]. The smaller A_{ex} values of CFA films are observed for $T_a = 300$ °C, where a decrease of M_s is also observed, most probably due to the lower crystalline quality and chemical order degree for the samples at this annealing temperature. It is worth remembering that the in-plane tetragonal distortion relaxes in all the samples at this T_a value.

The extracted effective magnetizations from the MS-FMR measurements are shown in Fig. 5(b) as a function of $1/t$ for the different T_a . Depending on t , two different regimes, separated by a critical thickness ($4 \text{ nm} < t_c < 7 \text{ nm}$, depending on T_a), can be distinguished. Indeed, for $t > t_c$, M_{eff} linearly increases with $1/t$ while it linearly decreases with $1/t$ for $t < t_c$. Therefore, a separate interpretation of the magnetic anisotropy must be made in the regions above and below t_c . According to the above structural investigation, $K_{v\perp}$ and $K_{s\perp}$ may include contributions of magnetocrystalline and magnetoelastic origin. In the case of epitaxial growth with a lattice misfit between the constituents, the particular form of strain encountered can contribute not only to $K_{v\perp}$ (regime I: $t < t_c$), but also to $K_{s\perp}$ (regime II: $t_c < t$) [18]. Therefore, in order to analyze the results of Fig. 5(a) and according to the model of Ref. [18], $K_{v\perp}$ and $K_{s\perp}$ are given by

$$\begin{aligned} K_{v\perp} &= K_{mc\perp} + K_{me,v\perp}^I, & \text{for regime I,} \\ K_{s\perp} &= K_{N\perp}, \end{aligned} \quad (6)$$

$$\begin{aligned} K_{v\perp} &= K_{mc\perp}, \\ K_{s\perp} &= K_{N\perp} + K_{me,s\perp}^{II}, \end{aligned} \quad \text{for regime II,} \quad (7)$$

where $K_{mc\perp}$ is the perpendicular magnetocrystalline anisotropy constant, $K_{me,v\perp}$, $K_{me,s\perp}$ are the perpendicular volume and interface strain anisotropy constants, and $K_{N\perp}$ is a Néel-type perpendicular interface anisotropy constant induced by the broken symmetry at the interfaces. According to this model, in region I, the influence of misfit strain appears as a volume contribution to the anisotropy, while it leads to an apparent interface contribution in regime II. The model suggests the occurrence of misfit dislocations during

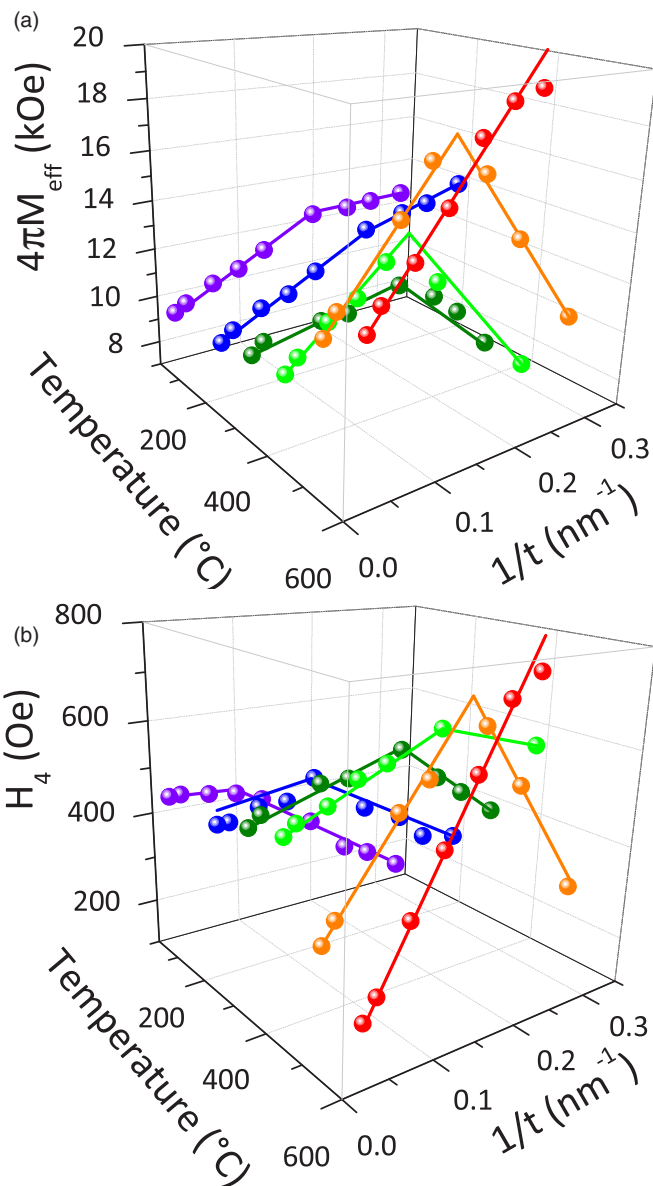


FIG. 5. 3D plot of the thickness dependence of (a) the effective magnetization ($4\pi M_{\text{eff}}$) and (b) fourfold anisotropy field, extracted from the fit of FMR measurements, of Co_2FeAl thin films annealed at different temperatures T_a . The solid lines are linear fits.

epitaxial film growth for $t \geq t_c$, as already encountered in Co_2MnSi [19] and Co_2FeAl [20] thin films grown on MgO. The estimation of this critical thickness can be predicted by theoretical models, with the most celebrated being the Matthews-Blakeslee (MB) [21,22] and People-Bean (PB) [23] models for the equilibrium theory. Because of their clarity and reasonably good agreement with experiments, these models, especially the PB one, have been widely accepted [24]. Being given the free lattice parameters, assuming 60° misfit dislocations, and by adopting the elastic coefficients given before, the MB and PB models give 2.4 and 5.2 nm for the critical thicknesses, respectively. This is in relatively good agreement with the value found from the MS-FMR measurements. It is generally admitted that the MB model provides a lower thermodynamic bound, based on equilibrium

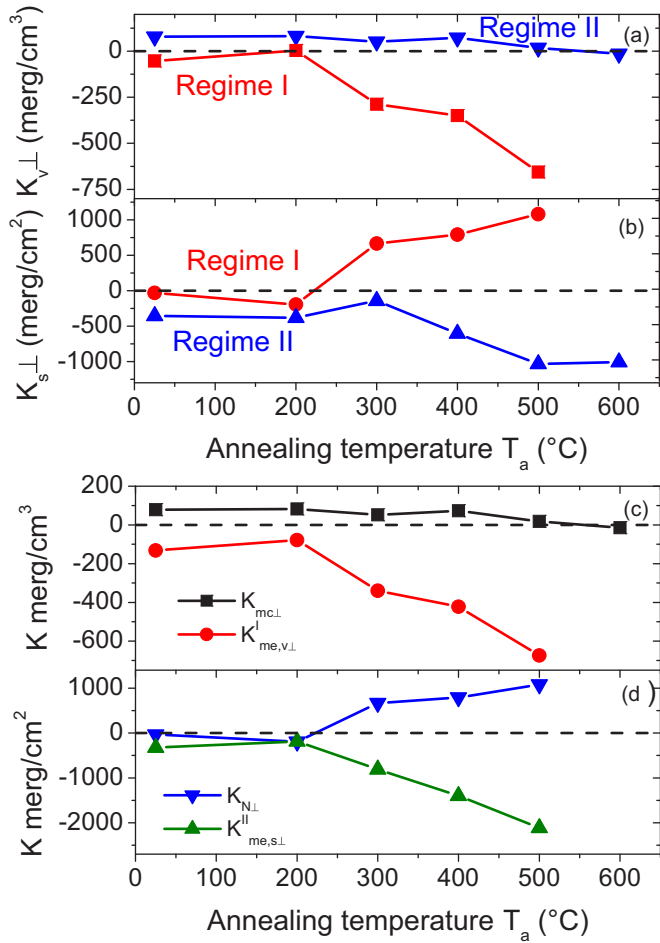


FIG. 6. Annealing temperature dependence of (a) the volume and (b) surface effective perpendicular anisotropy constants in the two regimes below and above the critical thickness. Variation of the different contributions of the (c) magnetocrystalline ($K_{me\perp}$) and the volume ($K_{me,v\perp}^I$) magnetoelastic and (d) the Néel-type interface ($K_{N\perp}$) and the surface ($K_{me,s\perp}^{II}$) anisotropy constants to the perpendicular anisotropy. The data in (c) and (d) were obtained from the measurements presented in (a) and (b) using Eqs. (6) and (7). Symbols refer to measurements and solid lines are used as guides to the eye. Dashed lines refer to grid lines for zero.

considerations, to the thickness at which coherency is lost [25]. The XRD measurements shown in Fig. 1 reveal that films down to 5 nm are relaxed, suggesting that the critical thickness is lower than 5 nm, in good agreement with the value given by the PB model and with the one determined from the thickness dependence of the effective magnetization deduced from the FMR measurements for the as-deposited and the annealed samples at 200, 300, and 600 °C presented in Fig. 5(a). For annealing temperatures (400 and 500 °C), the higher critical thickness deduced from the FMR measurements is due to the lack of intermediate thicknesses. More experimental data are needed to precisely determine the critical thickness as demonstrated in the case of samples annealed at 600 °C.

The linear fit of the measurements allows for the determination of the perpendicular surface and volume anisotropy constants for both regimes using Eqs. (3) and (4). Their variations as a function of T_a are shown in Figs. 6(a)

and 6(b). The volume constant [Fig. 6(a)], which has a magnetocrystalline origin in regime II according to Eq. (7), is positive over the whole range of T_a . It decreases slightly as T_a increases due to the enhancement of the chemical order with T_a , in agreement with the previously observed [17,26] trend, where the magnetocrystalline anisotropy would be higher in the A2 phase than in the B2 phase. The minimal value of $K_{v\perp}$ in this regime is obtained around an annealing temperature of 500 °C. In regime I, $K_{v\perp}$ is negative, much higher (in absolute value) than that of region II, and increases significantly for $T_a > 200$ °C, due to the magnetoelastic contribution, as predicted by Eq. (6). For the surface anisotropy [Fig. 6(b)], its absolute value increases with T_a in both regimes. However, compared to $K_{v\perp}$, its behavior versus T_a is different: It becomes positive for $T_a > 200$ °C in regime I, where it is pure Néel-type interface anisotropy [see Eq. (6)], while it is negative over the studied T_a range for regime II, due to the contribution of strain to the surface anisotropy, as predicted by Eq. (7). Therefore, we conclude that the linear thickness dependence of the effective magnetization is mainly governed by pure Néel-type surface interface anisotropy in region I, reinforcing a perpendicular easy axis, while it is given by the interface strain anisotropy favoring in-plane easy axes in regime II. The origin of this pure interface anisotropy can be attributed to the CFA/MgO interface due to the hybridization of the O 2*p* and metal-alloy 3*d* orbitals, according to calculations [27–29]. The enhancement of the surface anisotropy in regimes I and II can be correlated to the improvement of the interface quality due to the enhancement of the chemical order and to increases of the strain as T_a increases, respectively. It is worth mentioning that a significant effect of annealing temperatures on both volume and surface anisotropies is obtained for T_a above 200 °C. Using Eqs. (6) and (7) and the surface and volume anisotropy constant values presented in Figs. 6(a) and 6(b), the contributions of the magnetocrystalline, magnetoelastic, and Néel-type interface anisotropies to the surface and volume perpendicular anisotropies have been isolated. Their variations versus T_a , presented in Figs. 6(c) and 6(d), show that magnetoelastic anisotropy is negative and reinforces the in-plane easy axis. Its contributions, which are T_a dependent, to both volume and surface anisotropy are significant and are higher than those of the magnetocrystalline and the pure interface anisotropies. Therefore, to obtain perpendicular magnetized CFA thin films, the magnetoelastic anisotropy should be reduced to its minimum value or, preferably, high positive magnetoelastic anisotropy should be induced by properly choosing a suitable buffer or cap layer material such Ta [30] besides MgO.

The $1/t$ dependencies of the in-plane fourfold anisotropy fields, presented in Fig. 5(b), show a similar behavior as the effective magnetization over the investigated T_a range. However, this figure shows that the as-deposited and annealed samples at 200 °C present a different thickness dependence of the fourfold anisotropy compared to the samples annealed at other temperatures. We should stress that the effective magnetization is more sensitive to the three different anisotropy contributions when compared to the fourfold anisotropy and, therefore, its thickness dependence is similar for all annealing temperatures. In the case of the fourfold anisotropy field, since it is a second-order quantity and due to the lower above-mentioned anisotropy contributions at lower

temperature, the usual trend of the thickness dependence of the anisotropy is not respected. In fact, for thinner films ($t < t_c$: regime I), the fourfold anisotropy field linearly decreases with $1/t$ while it increases linearly for thicker samples ($t > t_c$: regime II). This critical thickness for H_4 is slightly different from that in the case of M_{eff} . Such a change in the in-plane fourfold magnetic anisotropy field with the thickness suggests a contribution of the in-plane biaxial lattice strain, besides the magnetocrystalline and the pure interface terms, to either volume (regime I) or surface (regime II) fourfold anisotropies, as mentioned above for perpendicular anisotropy. However, since an equibiaxial strain only induces a perpendicular anisotropy [31,32] considering only the second degree terms of magnetization components, it is necessary, in cubic or tetragonal symmetries, to expand the film magnetoelastic energy density up to the fourth degree in the direction cosines of the magnetization, whereas the expansion can be limited to the first order in strains, as mentioned in Ref. [33]. These fourth degree contributions in the expansion of the magnetoelastic energy allow one to justify the presence of a strain-induced fourfold magnetic anisotropy. Such a contribution of strain to the volume or surface fourfold anisotropies has been observed in the case of epitaxial Fe films [33]. Furthermore, annealed samples at 300°C show a different sign of the thickness dependence of the strain (see Fig. 2) while the thickness dependence of anisotropy is the same (Fig. 5). The measured anisotropy field presented in Fig. 5 is an effective field resulting from the contributions of surface, magnetocrystalline, and magnetoelastic anisotropies. These contributions depend on the temperature and therefore on structural properties. However, it is not straightforward to interpret correctly these observations. Indeed, it is worth mentioning that samples annealed at 300°C show a lower magnetization at saturation and a lower A_{ex} as revealed by Figs. 3(b) and 4(c), which makes a direct correlation between strain and anisotropy difficult.

The linear fit of the measurements allows for the determination of the perpendicular surface and volume anisotropy constants for both regimes using Eq. (5), as shown in Figs. 7(a) and 7(b). The volume anisotropy is positive in both regimes and favors the [110] easy axis. It increases (slightly decreases above 400°C) with increasing annealing temperatures in regime I (regime II). Figure 7(b) shows that the surface anisotropy term, which increases (in absolute value) with T_a , is negative (positive) and favors the [110] ([100]) direction as the easy axis. Using (6) and (7) (\perp should read as 4) and the surface and volume anisotropy constant values presented in Figs. 7(a) and 7(b), the contributions of the fourfold magnetocrystalline (K_{mc4}), magnetoelastic ($K_{me,v4}$ and $K_{me,s4}$), and the classical interface anisotropies (K_{N4}) to the surface and volume in-plane anisotropies have been separated. Their variations versus T_a presented in Figs. 7(c) and 7(d) show that magnetocrystalline anisotropy is positively reinforcing the in-plane [110] easy axis. It decreases as T_a increases due to the enhancement of the chemical order. In the same manner, the biaxial volume and surface magnetoelastic terms, which are T_a dependent, favor an in-plane [110] easy axis and constitute the most contribution to in-plane anisotropy. In contrast, the pure biaxial interface anisotropy is negatively reinforcing the [100] easy axis and increases (in an absolute

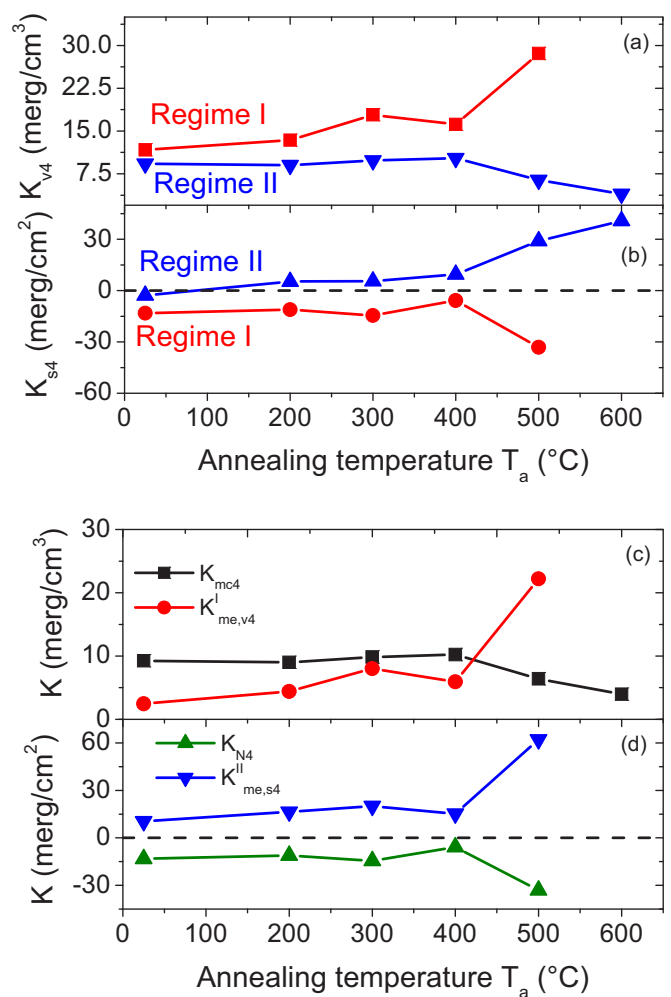


FIG. 7. Annealing temperature dependence of (a) the volume and (b) surface effective in-plane fourfold anisotropy constants in the two regimes below and above the critical thickness. Variation of the different contributions of the (c) magnetocrystalline (K_{me4}) and the volume ($K_{me,v4}^I$) magnetoelastic and (d) the Néel-type interface (K_{N4}) and the surface ($K_{me,s4}^{II}$) anisotropy constants to the in-plane fourfold anisotropy. The data in (c) and (d) were obtained from the measurements presented in (a) and (b) using Eqs. (6) and (7) by replacing \perp with 4. Symbols refer to measurements and solid lines are used as guides to the eye. Dashed lines refer to grid lines for zero.

value) as T_a increases due to the enhancement of the interface quality and the chemical order.

Various capping layers (Ta, V, and Cr) have been used to investigate their effects on perpendicular and in-plane anisotropies. For this, CFA films annealed at 450°C and having the same stack as the above studied films except for the cap layer have been used [30]. The existence of these two regimes in the effective magnetization and the in-plane fourfold anisotropy field has been observed only for MgO capped CFA films, suggesting an important role of the cap layer. Furthermore, all the perpendicular anisotropy constants of the various contributions are at least ten times higher than those of the in-plane ones.

Finally, it is worth mentioning that the in-plane uniaxial anisotropy fields, present in all the samples, do not show a clear

dependence versus t or T_a , making it difficult to identify their origin. We speculate that this uniaxial anisotropy is induced during the sample growth. Their values remain small compared to the fourfold anisotropy fields and do not exceed 30 Oe in most samples.

IV. CONCLUSION

Co₂FeAl films of various thicknesses ($3 \text{ nm} \leq t \leq 50 \text{ nm}$) and annealed at different temperatures were prepared by sputtering on (001) MgO substrates. They show epitaxial growing modes with the chemical order changing from the $B2$ to the $A2$ phase, as thickness and annealing temperatures decrease. The deduced in-plane and out-of-plane strains increase with annealing temperatures and vary linearly with the inverse thickness of the CFA films. Magnetic static characterizations revealed that both the magnetization at saturation and the magnetic dead layer increase with the annealing temperature. MS-FMR measurements consisting of measuring the excited mode frequency field dependencies and the angular evolutions of the resonance field have been used to extract the exchange stiffness constant, and the in-plane and perpendicular anisotropy fields. The exchange constant increases with the annealing temperature due to the enhancement

of the chemical order. The effective magnetization and the in-plane fourfold anisotropy field, present in all the samples, show a similar behavior versus $1/t$ where two different regimes, separated by a critical thickness, can be distinguished. For thinner films, they decrease linearly with $1/t$, while they increase linearly for film thicknesses greater than the critical thicknesses. This behavior has been interpreted through a model combining the magnetocrystalline, magnetoelastic, and pure interface anisotropies. Depending on the CFA thickness, the magnetoelastic anisotropy contributes to the volume or to the surface anisotropy for CFA thicknesses below or above the critical thicknesses, respectively. The annealing temperature dependence of the different contributions and their effect on the easy axis anisotropies have been studied.

ACKNOWLEDGMENTS

M.S.G. acknowledges the financial support of UEFIS-CDI through PN-II-RU-TE-2014-4-1820 SPINCOD Research Grant No. 255/01.10.2015. C.T. acknowledges the Exploratory Research Project, SPINTAIL PN-II-ID-PCE-2012-4-0315, No. 23/29.08.2013, and POS CCE ID. 574, code SMIS-CSNR 12467, for financial support.

-
- [1] H. C. Kandpal, G. H. Fecher, and C. Felser, *J. Phys. D* **40**, 1507 (2007).
 - [2] R. A. de Groot, F. M. Mueller, P. G. van Engen, and K. H. J. Buschow, *Phys. Rev. Lett.* **50**, 2024 (1983).
 - [3] T. Graf, C. Felser, and S. P. Parkin, *Prog. Solid State Chem.* **39**, 1 (2011).
 - [4] D. C. Ralph and M. D. Stiles, *J. Magn. Magn. Mater.* **320**, 1190 (2008).
 - [5] S. Trudel, O. Gaier, J. Hamrle, and B. Hillebrands, *J. Phys. D* **43**, 193001 (2010).
 - [6] W. H. Wang, E. Liu, M. Kodzuka, H. Sukegawa, M. Wojcik, E. Jedryka, G. H. Wu, K. Inomata, S. Mitani, and K. Hono, *Phys. Rev. B* **81**, 140402(R) (2010).
 - [7] W. H. Wang, H. Sukegawa, and K. Inomata, *Phys. Rev. B* **82**, 092402 (2010).
 - [8] M. Belmeguenai, H. Tuzcuoglu, M. S. Gabor, T. Petrisor, Jr., C. Tiusan, D. Berling, F. Zighem, T. Chauveau, S. M. Chérif, and P. Moch, *Phys. Rev. B* **87**, 184431 (2013).
 - [9] H. Ulrichs, B. Lenk, and M. Münzenberg, *Appl. Phys. Lett.* **97**, 092506 (2010).
 - [10] K. Yakushiji, K. Norma, T. Saruya, H. Kubota, A. Fukushima, T. Nagahama, S. Yuasa, and K. Ando, *Appl. Phys. Express* **3**, 053003 (2010).
 - [11] Z. M. Zeng, P. Khalili Amiri, G. Rowlands, H. Zhao, I. N. Krivorotov, J.-P. Wang, J. Langer, K. Galatsis, K. L. Wang, and H. W. Jiang, *Appl. Phys. Lett.* **98**, 072512 (2011).
 - [12] S. Picozzi, A. Continenza, and A. J. Freeman, *Phys. Rev. B* **69**, 094423 (2004).
 - [13] W. H. Butler, X.-G. Zhang, T. C. Schulthess, and J. M. MacLaren, *Phys. Rev. B* **63**, 054416 (2001).
 - [14] M. S. Gabor, T. Petrisor, Jr., C. Tiusan, M. Hehn, and T. Petrisor, *Phys. Rev. B* **84**, 134413 (2011).
 - [15] H. J. Elmers, S. Wurmehl, G. H. Fecher, G. Jakob, C. Felser, and G. Schönhense, *Appl. Phys. A* **79**, 557 (2004).
 - [16] M. Belmeguenai, H. Tuzcuoglu, M. S. Gabor, T. Petrisor, Jr., C. Tiusan, F. Zighem, S. M. Cherif, and P. Moch, *J. Appl. Phys.* **115**, 043918 (2014).
 - [17] S. Trudel, G. Wolf, J. Hamrle, B. Hillebrands, P. Klaer, M. Kallmayer, H. J. Elmers, H. Sukegawa, W. Wang, and K. Inomata, *Phys. Rev. B* **83**, 104412 (2011).
 - [18] M. T. Johnson, P. J. H. Bloemenz, F. J. A. den Broeder, and J. J. de Vries, *Rep. Prog. Phys.* **59**, 1409 (1996).
 - [19] G. Ortiz, A. García-García, N. Biziere, F. Boust, J. F. Bobo, and E. Snoeck, *J. Appl. Phys.* **113**, 043921 (2013).
 - [20] M. S. Gabor, C. Tiusan, T. Petrisor, Jr., T. Petrisor, M. Hehn, Y. Lu, and E. Snoeck, *J. Magn. Magn. Mater.* **347**, 79 (2013).
 - [21] J. W. Matthews and A. E. Blakeslee, *J. Cryst. Growth* **27**, 118 (1974).
 - [22] J. W. Matthews and A. E. Blakeslee, *J. Cryst. Growth* **32**, 265 (1976).
 - [23] R. People and J. Bean, *Appl. Phys. Lett.* **47**, 322 (1985).
 - [24] F. Y. Huang, *Phys. Rev. Lett.* **85**, 784 (2000).
 - [25] Y. B. Chen, H. P. Sun, M. B. Katz, X. Q. Pan, K. J. Choi, H. W. Jang, and C. B. Eom, *Appl. Phys. Lett.* **91**, 252906 (2007).
 - [26] O. Gaier, J. Hamrle, S. J. Hermsdoerfer, H. Schulthei, B. Hillebrands, Y. Sakuraba, M. Oogane, and Y. Ando, *J. Appl. Phys.* **103**, 103910 (2008).
 - [27] H. X. Yang, M. Chshiev, B. Dieny, J. H. Lee, A. Manchon, and K. H. Shin, *Phys. Rev. B* **84**, 054401 (2011).
 - [28] A. Hallal, H. X. Yang, B. Dieny, and M. Chshiev, *Phys. Rev. B* **88**, 184423 (2013).
 - [29] J. Okabayashi, J. W. Koo, H. Sukegawa, S. Mitani, Y. Takagi, and T. Yokoyama, *Appl. Phys. Lett.* **105**, 122408 (2014).

- [30] M. Belmeguenai, M. S. Gabor, T. Petrisor, Jr., F. Zighem, S. M. Chérif, and C. Tiusan, *J. Appl. Phys.* **117**, 023906 (2015).
- [31] M. Gueye, F. Zighem, M. Belmeguenai, M. S. Gabor, C. Tiusan, and D. Faurie, *J. Phys. D: Appl. Phys.* **49**, 145003 (2016).
- [32] M. Gueye, F. Zighem, M. Belmeguenai, M. S. Gabor, C. Tiusan, and D. Faurie, *J. Phys. D: Appl. Phys.* **49**, 265001 (2016).
- [33] N. Tournerie, P. Schieffer, B. Lépine, C. Lallaizon, P. Turban, and G. Jézéquel, *Phys. Rev. B* **78**, 134401 (2008).